COMSAT
Technical Review
Volume 1 Number 1, Fall 1971



**Index: INTELSAT IV, propellant tanks, sloshing, spacecraft, spin stabilization**

# EXPERIMENTAL INVESTIGATIONS ON THE FUEL SLOSH OF DUAL-SPIN SPACECRAFT

ERNESTO R. MARTIN

## ABSTRACT

Energy dissipated by vibrating components on the spinning rotor of a dual-spin spacecraft, such as the INTELSAT IV communications satellite, has a destabilizing effect on the dynamics of the vehicle. Experimental investigations to determine fuel slosh energy dissipation revealed unexpectedly turbulent fluid motions in the sphere-cone propellant tanks of INTELSAT IV. The liquid motion was observed inside a spinning tank subjected to angular oscillations similar to those of the spacecraft. Earlier tests in which the spinning tank was subjected to rectilinear vibration, but similar linear accelerations, had resulted in calm, rigid-body, pendulous fluid motion. It was found that the turbulent fluid motion is excited when a spinning tank is subjected to angular oscillations about an axis which is not parallel to the symmetry axis of the tank.

## INTRODUCTION

A dual-spin satellite consists of a nonspinning platform coupled, through a bearing interface, to a rotor which spins about the minimum moment-of-inertia axis of the spacecraft. This unique design concept embodies several characteristics desirable for synchronous communications satellites. Among these are spin stabilization to provide gyroscopic stiffness and a nonspinning platform from which directional antennas can beam the communications power toward the earth.

In order to keep the antenna beams directed toward the earth, two conditions are necessary:

a. the platform on which the antennas are mounted must be kept properly despun relative to the earth, and

b. the spin axis of the rotor must remain inertially fixed.

---

This paper is based upon work performed under the sponsorship of the International Telecommunications Satellite Consortium (INTELSAT). Any views expressed in this paper are not necessarily those of INTELSAT.

The first condition is achieved through earth sensors and an internal control system which governs the torque of an electric motor housed in the bearing interface between the platform and the rotor. The second condition is dependent on the spacecraft dynamic stability. If the spacecraft is nutating, the coning motion of the spin axis prevents the antennas from pointing at desired targets on the earth. In the absence of external forces, the nutation angle, $\theta$, is given by

$$\theta = \theta_0 e^{-t/\tau_s} \tag{1}$$

where $t$ = time

$\theta_0$ = nutation angle at time zero

$\tau_s$ = spacecraft time constant.

For the spacecraft to be stable, $\tau_s$ must be positive.

Using energy sink methods, other investigators [1], [2] had earlier derived the necessary conditions for $\tau_s$ to be positive. For a dual-spin vehicle with a frictionless bearing interface and axisymmetric rotor and despun platform, the necessary condition is

$$\dot{E}_r < \left[\frac{1 - (I_r/I_T)}{I_r/I_T}\right] \dot{E}_d \tag{2}$$

where $\dot{E}_r$ = the rate of energy dissipated by vibrating components in the rotor

$I_r$ = the moment of inertia of the rotor about the spin axis

$I_T$ = the moment of inertia of the spacecraft about a transverse axis

$\dot{E}_d$ = the rate of energy dissipated by vibrating components on the despun platform.

Energy dissipating passive nutation dampers mounted on the platform can provide the necessary $\dot{E}_d$. Stability is assured whenever equation (2) is satisfied.

Indeed, the first dual-spin spacecraft ever launched, TACSAT, exhibited an undamped nutation of about 1° [3] induced by excessive energy dissipation in its rotor. Soon afterward, the firm of Harrington, Davenport and Curtis, Inc., consultants to COMSAT, initiated a study to predict the stability of the INTELSAT IV communications satellite (Figure 1) which was being designed by the Hughes Aircraft Company. It was found that the major uncertainty was the magnitude of the energy dissipated by the hydrazine liquid propellant in the four sphere-cone



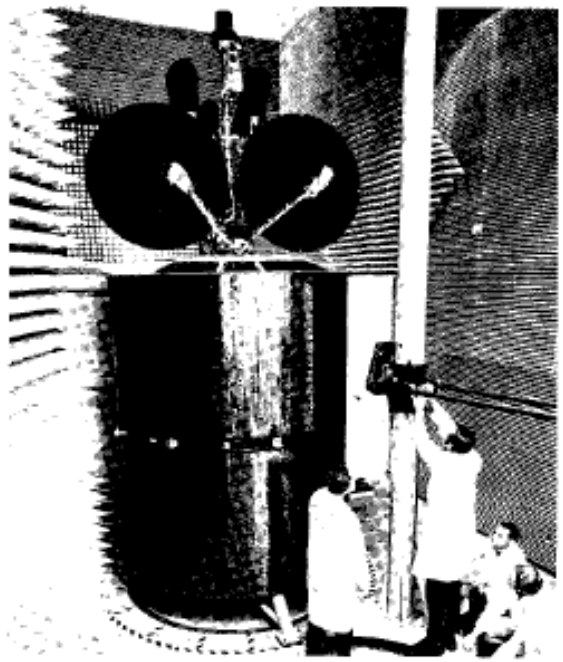

*Figure 1. INTELSAT IV*

tanks housed in the rotor. Therefore, it was recommended that the energy dissipation rate ($\dot{E}$) of the fuel slosh be investigated.

While intensive analytical studies were continued by Harrington, Davenport and Curtis, Inc., an experimental program was initiated at COMSAT Laboratories. Hughes Aircraft Company also initiated experimental investigations to measure the fuel slosh $\dot{E}$ on INTELSAT IV. The Hughes program used an air-ball-test technique similar to the one Hughes had previously used for TACSAT and ATS-E. This paper, however, reports only the work performed at COMSAT Laboratories. COMSAT's objective was to measure the $\dot{E}$ of the fuel in an INTELSAT IV tank subjected to motions similar to those it experiences on the spacecraft.

## TEST PROGRAM: LINEAR MOTION

A test fixture was desired which would simulate the spacecraft excitation on the tank. A dynamic analysis of a general dual-spin spacecraft was performed and is presented in Appendix A. The body-fixed co-

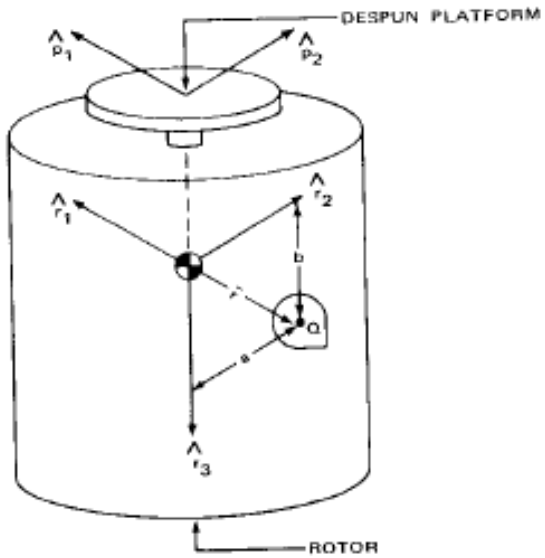


*Figure 2. Dual-Spin Spacecraft Showing Coordinate System Used*

ordinate system and overall configuration are shown in Figure 2. The sphere-cone tank has the outlet at the cone apex to allow full propellant depletion in both ground and orbital conditions. The center of the spherical section is defined as the center of the tank and labeled Q. The origin of the coordinate system is coincident with the center of gravity (CG) of the spacecraft. The position vector from the origin to the tank center is

$$\bar{r}_Q = a\hat{r}_2 + b\hat{r}_3 \tag{3}$$

where $\hat{r}_2$ and $\hat{r}_3$ are unit vectors in the direction shown in Figure 2. The linearized acceleration experienced by $Q$ is equal and opposite to $\bar{a}_Q$, which is derived with respect to an inertial frame in Appendix A; i.e.,

$$\begin{aligned} -\bar{a}_Q = {} & \hat{r}_1(b\sigma^2\omega_s^2\theta \sin \lambda' t) \\ & + \hat{r}_2(-b\sigma^2\omega_s^2\theta \cos \lambda' t + a\omega_s^2) \\ & + \hat{r}_3[a\sigma\omega_s^2\theta(\sigma - 2) \cos \lambda' t] \end{aligned} \tag{4}$$

where $\sigma$ is the moment-of-inertia ratio $(I_r/I_T)$, $\omega_s$ is the rotor spin rate, and $\lambda'/2\pi$ is the rotor nutation frequency given by



$$\lambda' = (-1 + \sigma)\omega_s. \tag{5}$$

The first spinning test selected is shown in Figure 3. A plexiglass INTELSAT IV tank is driven with linear sinusoidal motion by the onboard motor and cam arrangement at an angle $\psi$ from the horizontal. This angle is chosen so that the constant acceleration, which is made up of gravity and the centripetal acceleration, is perpendicular to the direction of motion. The tank is also canted by an angle $\psi$ to preserve the same relationship between liquid free surface and tank geometry that exists in the spacecraft. The liquid is viewed by an onboard television camera with variable mounting and lenses, remotely monitored on a TV screen, and recorded on a video tape recorder. Instrumentation includes a tachometer, a pulse-per-revolution calibrator, a linear displacement transducer, and an accelerometer with its sensing axis parallel to the $\hat{r}_1$ axis. Slip rings allow transfer of power and signals to and from the table.

When the linear motion of the tank has an amplitude $X$ and time function $\cos \lambda' t$ at an angle $\psi$ from the horizontal, and when the spin rate is $\omega_s$, the linearized acceleration experienced by the center of the tank in the presence of the gravitational acceleration, $g$, is found to be (Appendix B)

$$\begin{aligned} g\hat{r}_2 - \bar{a}_Q = {} & [2X\omega_s\lambda' \cos \psi \sin \lambda' t]\,\hat{r}_1 \\ & + [(\lambda'^2 + \omega_s^2)\,X \cos \psi \cos \lambda' t + a\omega_s^2]\,\hat{r}_2 \\ & + [g - X\lambda'^2 \sin \psi \cos \lambda' t]\,\hat{r}_3. \end{aligned} \tag{6}$$

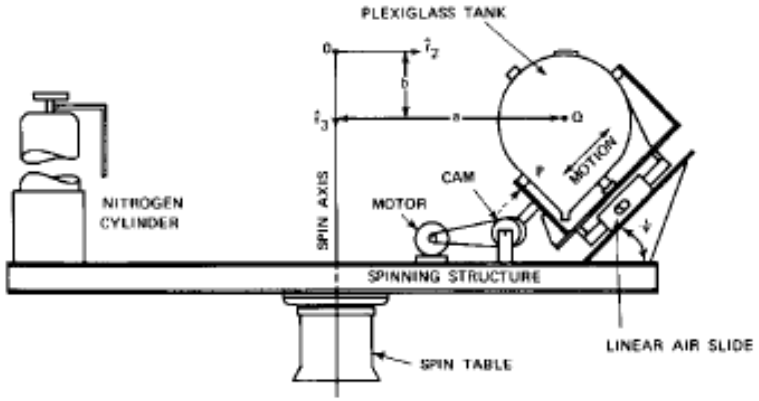


*Figure 3. Linear Motion Spinning Test Fixture*

Notice that, although the tank's motion is in the $\hat{r}_2$, $\hat{r}_3$ plane, there is an acceleration component in the $\hat{r}_1$ direction because of Coriolis effects.

Table 1 is a numerical comparison of these harmonic accelerations with those of INTELSAT IV (where $a = 23.5$ in., $b = 11$ in., and mid-life $\sigma = 0.33$) for a spin speed of 60 rpm, 1° nutation, $\phi$ equal to the test value of 73°, and the $X$ amplitude chosen so that the $\hat{r}_3$ acceleration is the same as that on the spacecraft. In the $\hat{r}_1$, $\hat{r}_2$ directions, the accelerations on the test fixture are about 10 times greater than they are on the spacecraft and in the opposite direction. Notice, however, that the amplitude and phase relationship between the $\hat{r}_1$ and $\hat{r}_2$ accelerations on the test fixture is similar to the relationship between the $\hat{r}_1$ and $\hat{r}_2$ accelerations on the spacecraft. Therefore, the test fixture, which is thought to provide an adequate simulation of the spacecraft's linear accelerations, yields conservative results because of the much greater amplitude of the $\hat{r}_1$ and $\hat{r}_2$ excitations.

TABLE 1. LINEARIZED ACCELERATIONS FOR THE LINEAR MOTION TEST FIXTURE AND THE SPACECRAFT

| Direction | Linearized Acceleration, in./sec² | |
|---|---|---|
| | Linear Motion Spinning Test | Spacecraft |
| $\hat{r}_1$ | $-8.14 \sin \lambda' t$ | $0.83 \sin \lambda' t$ |
| $\hat{r}_2$ | $8.81 \cos \lambda' t$ | $-0.83 \cos \lambda' t$ |
| $\hat{r}_3$ | $-8.92 \cos \lambda' t$ | $-8.92 \cos \lambda' t$ |

While the fixture was being designed and fabricated, one of the INTELSAT IV tanks was subjected to nonspinning unidirectional vibration of amplitudes and frequencies typical of the spacecraft. The objectives of these preliminary tests were to evaluate the effect of the sphere-cone tank shape on fuel $\dot{E}$ and to obtain baseline $\dot{E}$ values. The spherical section of the tank had a diameter of 17.4 inches and the conical section had an angle of 86° (axis to wall equals 43°, as shown by the tank of Figure 3).

The fluid $\dot{E}$ measured in the vibration tests [4] was in reasonably good agreement with analytical models which assumed rigid-body fluid motion. The damping ratio of the liquid* was similar to that of a fluid in a sphere of the same diameter.

* Water was used for all the tests because its viscosity, density, and surface tension are very similar to those of hydrazine.



**Results: Fluid Motion**

The first series of tests was designed to study the fluid behavior and to compare it with that predicted by the rigid-body analysis. The camera was located to view the entire liquid. Free-surface motion was observed by introducing numerous floating particles, while bulk motion was studied by dropping dye on the surface and observing its migration and motion below the surface.

Throughout the range of spin speed and nutation frequency of INTELSAT IV, the liquid was very calm. Surface particles exhibited rectilinear oscillations at the driving frequency with amplitudes in the immediate neighborhood of the tank amplitude. The dye below the surface appeared almost motionless and its migration through the liquid was very slow. As would be expected, when the driving frequency approached the natural frequency of the fluid (about three times greater than the nutation frequency), its motion increased significantly.

**Results: Measurement of Fluid $\dot{E}$**

The camera is positioned to view closely point $P$ of the tank in the direction shown by the dashed arrow of Figure 3. By measuring the oscillation amplitude of the liquid surface where it contacts the tank wall at $P$ for different driving frequencies and tank amplitudes, one can plot the vibrational potential energy ($E_p$) of the liquid as a function of driving frequency and tank amplitude. Tests in which the tank is abruptly stopped and the decay history of the liquid oscillation is recorded permit calculations of its time constant, $\tau$, and the natural frequency, $\omega_n$. Since the fluid exhibits rigid-body pendulous motion, its energy dissipation rate is given by

$$\dot{E} = \frac{2E_p}{\tau}\left(\frac{\lambda'}{\omega_n}\right)^2. \tag{7}$$

This is the equation used to compute the fuel slosh $\dot{E}$ from the data obtained from the described test sequences [4].

The tests performed were limited to a propellant tank which was one-third full (35 lbs.) because the $\dot{E}$ is fairly independent of mass when the fluid exhibits pendulous motion and when the excitation frequency is smaller than the liquid's natural frequency. The results of $\dot{E}$ vs. $\lambda'$ for four discrete nutation angles are presented in Figure 4 for a spin speed of 48 rpm. Limitations in the equipment did not allow measurements at different spin speeds. The driving frequency, $\lambda'$, in terms of the inertia ratios for INTELSAT IV from start of life to end of life, is presented on the abscissa. The energy dissipation rate has been normalized by dividing it by the nutation angle squared.

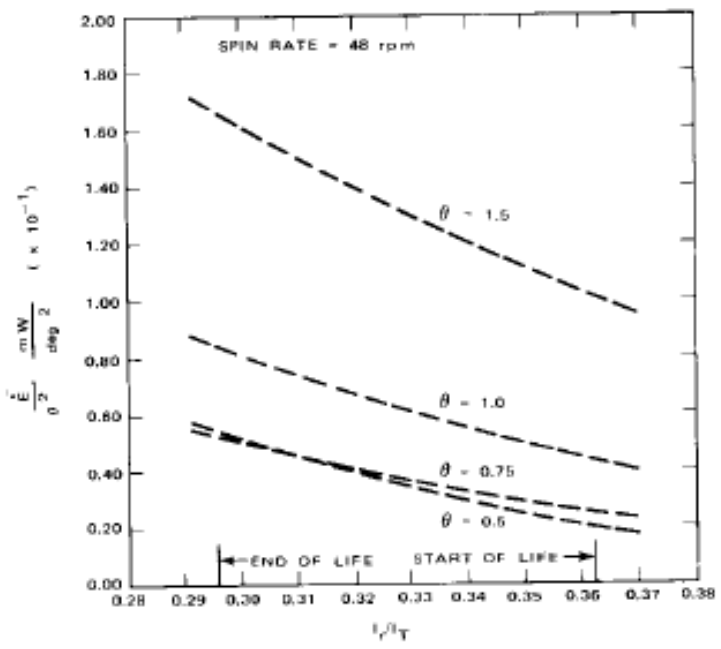


*Figure 4. Results of Fuel Slosh $\dot{E}$ on the Linear Motion Fixture*

The stability margins calculated for INTELSAT IV using the preceding fuel slosh $\dot{E}$ results were found to be adequate. There was some concern, however, that the linear motion to which the tank was subjected did not provide a sufficiently good simulation of the motion which the tank experiences on the spacecraft.

Because the spacecraft CG in inertial space is stationary, the tank should exhibit arc motion instead of the linear motion to which it was subjected in the tests. The arc motion may be separated into a translation of the center of the tank and a rotation* of the tank relative to its center. A kinematic analysis, developed in spherical polar coordinates (and briefly described in the next section), was used to gain some insight into the tank's motion on the spacecraft. It confirmed the existence of angular oscillatory components of motion. The effect which these oscillatory tank rotations would have on the liquid's behavior was discussed with fluid mechanics consultants and examined through the review of

* The term "rotation" of the tank will continue to be used in this context and should not be confused with spinning of the tank.



pertinent literature [6], [7]. The possibility was raised [8] that the presence of the tank cone and the interaction between the angular oscillation axes and the spin axis may lead to localized fluid perturbations and nonuniform flow with considerably higher $\dot{E}$.

A test which would subject the tank to oscillations which were more representative of the spacecraft motion was desired.

## TEST PROGRAM: ANGULAR MOTION

The first task in designing a new fixture was to establish the motion of the tank on the satellite. Since the results from the kinematic analysis of the spacecraft were used, they are briefly described here.

A reference frame, $T$, spinning about an inertially fixed axis, $\hat{t}_3$ (which coincides with the vehicle's total angular momentum vector), at a prescribed constant rate (which, for small nutation angles, is nearly identical to the spacecraft's spin rate) is chosen. In a spherical coordinate system in which the origin is at the spacecraft CG (Figure 5), the motion of the tank center, $Q$, as seen from the $T$ reference frame, can be expressed in terms of the angular displacements $\alpha$ and $\beta$. The $\alpha$ motion was found to be given by

$$\alpha = \alpha_0 - \theta \cos \lambda' t \tag{8}$$

where $\alpha_0$ is the value of $\alpha$ in the absence of nutation; i.e.,

$$\alpha_0 = \cos^{-1} \frac{b}{r} = \sin^{-1} \frac{a}{r}. \tag{9}$$

No second-order terms exist in $\alpha$. The equation for $\beta$ contains a second-order term, but as shown in Section 5.3 of Reference [4], its amplitude is insignificant. For small nutation angles, $\beta$ may be expressed as

$$\beta = \frac{\pi}{2} - \frac{b}{a} \theta \sin \lambda' t. \tag{10}$$

The dependence of the amplitude on $b/a$ means that there is another angular oscillation about the $\hat{t}_2$ axis.

The spinning angular motion test fixture which was designed to subject the tank to these motions is shown in Figure 6 and was completed in October 1970. (The launch of the first INTELSAT IV spacecraft was scheduled for December 1970.) The table, spinning at a constant rate, is analogous to the $T$ reference frame; $\hat{t}_3$ is coincident with the spin axis. A tubular structure supports the tank and is hinged through a pair of bearings. When the tank is in its undisplaced (null) position, the radius vector to $Q$ is of the form $a\hat{t}_2 + b\hat{t}_3$. Thus, $\alpha_0$ and the same

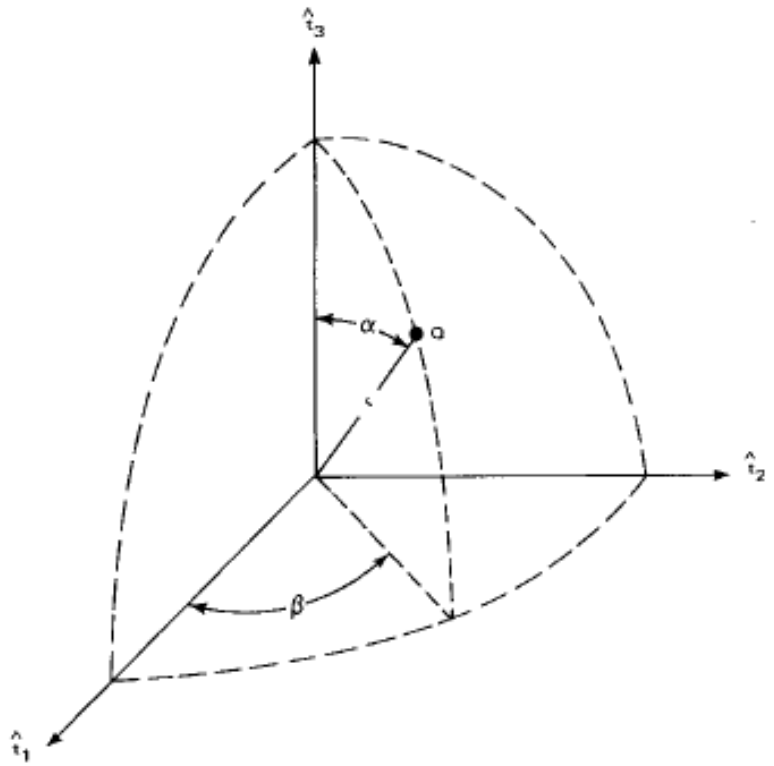


*Figure 5. Spherical Coordinate System Used for Kinematic Analysis*

geometry are maintained. The $\alpha$ motion is achieved through an onboard motor and an off-center crank arrangement which drives the tank in an arc of amplitude $\theta$ and frequency $\lambda'$.

If the spin motor is producing a constant torque, the magnitude of the spin speed will exhibit a small sinusoidal variation of frequency $\lambda'$ because of the moment-of-inertia change of the fixture as the tank describes its arc motion. This small ripple, superimposed on the mean spin rate, indicates that an observer spinning at the mean spin rate (the equivalent of the $T$ reference frame) will see the tank exhibit an angular oscillation of nutation frequency about the spin axis. This $\beta$ motion is 90° out of phase with the $\alpha$ motion, as on the spacecraft, but its ampli-



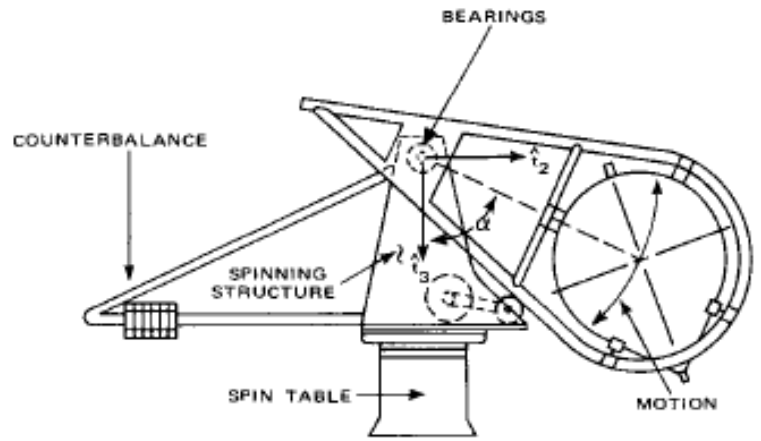


*Figure 6. Angular Motion Spinning Test Fixture*

the amplitude ranged between the spacecraft amplitude and twice that value. Since the initial objective of this fixture was to simulate the oscillatory motions of the tank on the spacecraft, a dynamic analysis was performed to compare the linearized accelerations to those on the spacecraft. The next section presents the results of this analysis.

**Angular Motion Test Fixture Accelerations**

The $\alpha$ arc motion to which the tank is subjected by the motor crank arrangement is of the form,

$$\alpha = \alpha_0 - \theta \cos \lambda' t \tag{11}$$

which is the same as that on the spacecraft [equation (8)]. The instantaneous position vector to $Q$ is

$$\bar{r}_Q = (r \sin \alpha)\, \hat{t}_2 + (r \cos \alpha)\, \hat{t}_3 . \tag{12}$$

The angular velocity of the fixture is

$$\bar{\omega} = (\omega_s + \omega_{sr} \cos \lambda' t)\, \hat{t}_3 \tag{13}$$

where $\omega_{sr}$ is the magnitude of the spin ripple.

The same method used in Appendix B is used to find the acceleration of $Q$ in $\hat{t}_1$, $\hat{t}_2$, $\hat{t}_3$ coordinates. A transformation matrix is then used to change the acceleration to the $\hat{r}_1$, $\hat{r}_2$, $\hat{r}_3$ coordinate system fixed in the tank. The final result for the linearized accelerations felt by the center of the tank is

$$g\hat{i}_3 - \bar{a}_{0'} = [(2b\theta\omega_s\lambda' - a\omega_{sr}\lambda')\sin\lambda' t]\,\hat{r}_1 + [F_1\cos\lambda' t + a\omega_s^2]\,\hat{r}_2 + [a\theta\omega_s^2\sigma(\sigma - 2)\cos\lambda' t + g]\,\hat{r}_3 \quad (14)$$

where
$$F_1 = -\theta[(\lambda'^2 + \omega_s^2)b - g] + 2a\omega_s\omega_{sr}\,. \quad (15)$$

A comparison of the time-dependent accelerations of this fixture with those experienced by the tank on the spacecraft for a nutation angle of 1°, a spin rate of 60 rpm, an inertia ratio of 0.33, and a fixture spin ripple of 0.3 rpm is presented in Table 2. When the accelerations in this table are compared to the accelerations of the first test fixture (Table 1), it can be seen that the new test fixture provides somewhat better simulation of the accelerations, as well as excellent motion simulation.

TABLE 2. LINEARIZED ACCELERATIONS FOR THE ANGULAR MOTION TEST FIXTURE AND THE SPACECRAFT

| Direction | Linearized Acceleration, in./sec² | |
|---|---|---|
| | Angular Motion Spinning Test | Spacecraft |
| $\hat{r}_1$ | $-7.05 \sin \lambda' t$ | $0.83 \sin \lambda' t$ |
| $\hat{r}_2$ | $5.04 \cos \lambda' t$ | $-0.83 \cos \lambda' t$ |
| $\hat{r}_3$ | $-8.92 \cos \lambda' t$ | $-8.92 \cos \lambda' t$ |

## Test Results

The test fixture was dynamically balanced to operate at 45, 55, and 70 rpm and at liquid weights of 20, 35, and 60 pounds with the magnitude and location of counterweights recorded for all of the nine possible conditions. As the very first test was being run, it immediately became evident that the nature of the liquid motion had drastically changed. Small but highly energetic vortices were apparent on the free surface of the fluid. The localized vortices were so strong that they deformed the otherwise smooth, free surface and created dimples which protruded into the liquid. These vortices were not stationary, but moved around the surface in circles, having more vorticity at some points than at others. Floating particles were introduced in the liquid to better observe the surface activity. The surface particles exhibited energetic oscillations which sometimes had amplitudes as large as the radius of the tank.



Even more surprising was the behavior of the bulk of the fluid. Dye-injection techniques revealed high fluid velocities below the free surface. Dye dropped on the surface was literally sucked below the surface and energetic turbulent mixing spread the dye throughout the liquid, all in an interval of between 2 and 10 seconds.

The technique used in the linear motion fixture for measuring fuel $\dot{E}$ could not be used now because the liquid motion was no longer similar to that of a rigid body. It was decided to make a qualitative evaluation of surface particle motion and dye diffusion in order to examine the dependence of the liquid activity on spin speed, nutation frequency, nutation angle, and amount of fill. The liquid turbulence increased when any of these parameters was increased independently. No step change in liquid behavior as a function of any of these parameters was noticed; although reduced, the turbulence persisted even at very small nutation angles, such as one-tenth of a degree.

As the numerous tests were performed with different dye injection locations and the liquid's motion was recorded on videotape, a clearer understanding of the motion beneath the surface was obtained. From real-time and videotape analysis of the dye dispersion, it appeared that there was a mass flow toward the cone apex along and immediately adjacent to the cone axis. The mass of liquid then flowed away from the cone closer to the walls.

Figure 7 is a representation of a cross-section of the tank showing

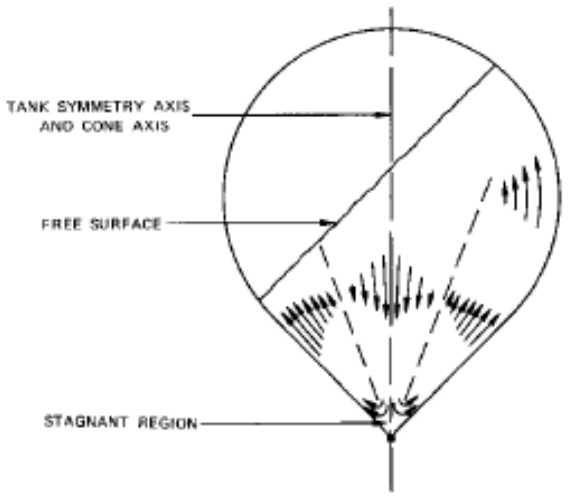


*Figure 7. Turbulent Fluid Motion Within the Bulk of the Liquid*

the apparent liquid motion. The arrows give an indication of relative fluid velocity. Pressurized injection of dye at the apex of the cone (which is the tank outlet) remained confined to a small volume at the apex instead of diffusing throughout the liquid; this indicated the presence of a stagnant region. When the dye was pressurized even further so that it squirted through the stagnant area into the bulk, it exhibited the motion indicated in Figure 7.

A plexiglass spherical tank of similar size was fabricated and subjected to tests. The liquid motion was calm, exhibiting rigid-body pendulous motion. The shape of the tank therefore appeared to have an important effect on the liquid motion.

The air ball tests conducted by Hughes Aircraft Company, the spacecraft contractor, successfully quantized the turbulent fluid motion energy dissipation in the INTELSAT IV tanks [5]. The measured $\dot{E}$ values were obviously greater than had been predicted by the rigid-body analytical model. (For a spherical tank, they found that the $\dot{E}$ was between 8 and 10 times smaller than for the sphere-cone tank.) To compensate for the larger fuel $\dot{E}$, the contractor incorporated design modifications on INTELSAT IV to increase the stability margins. The satellite, launched January 25, 1971, has demonstrated passive nutational stability in both transfer and synchronous orbits.

## INVESTIGATIONS TO EXPLAIN TURBULENT FLUID MOTION

Following the successful launch of INTELSAT IV, an investigation was started in an attempt to explain the cause of the turbulent fluid motion. The dynamic excitation of the tank and the tank geometry appeared to be equally important in influencing the liquid motion. In order to further investigate the effect of dynamic excitation, attention was directed toward the difference between the linear motion fixture and the angular motion fixture. Although the linearized accelerations acting on the tank were about the same for both tests and the liquid properties were the same, two differences could be cited. The angular motion tests subjected the tank to arc motion and spin ripple, while the other test subjected the tank to rectilinear motion and little, if any, ripple.

In order to investigate the influence of the spin ripple on the fluid behavior, an open-loop control system (called the electronic ripple modulator) was designed and assembled to vary the spin ripple, $\omega_{sr}$, on the angular motion fixture. This was accomplished by using the angular displacement transducer signal (which has a voltage proportional to the $\alpha$ motion) as a phase reference to modulate the voltage to the spin motor. Hence, $\omega_{sr}$ was no longer dependent on the fixture's moment-of-inertia change caused by the $\alpha$ motion, but could be set independently.



Tests performed with different values of spin ripple, and with no spin ripple, exhibited little difference in the fluid's motion. Although the spin ripple appeared to have little influence on fluid behavior, the linear motion test fixture was placed back in operation and subjected to tests with large values of spin ripple. As in the earlier tests with that fixture, the fluid remained calm and exhibited rigid-body, pendulous motion. Of the dynamic excitation on the tank, it appeared, therefore, that the arc motion and not the spin ripple was responsible for the fluid turbulence.

The preliminary conclusion was that turbulent fluid behavior is excited inside a spinning sphere-cone tank subjected to oscillatory arc motion, but not in a spherical tank. Further analysis of the results, however, seemed to indicate that such a general conclusion was inaccurate. The liquid had remained calm when the sphere-cone tank on the linear motion test fixture had been subjected to spin ripple, a condition which excited the tank with arc motion about the spin axis. In other words, the linear motion test fixture with spin ripple indeed subjected the tank to an arc motion, the $\beta$ motion, and yet the fluid exhibited rigid-body calm motion.

Seeking an explanation of this inconsistency, we recognized that the spin axis about which these angular oscillations occurred was parallel to the tank's symmetry axis (Figure 3). This led the author to hypothesize that turbulent fluid motion is excited in a spinning tank only when the tank is subjected to angular oscillations about an axis which is not parallel to its symmetry axis. This hypothesis was not only consistent with all of the experimental results (including those from the sphere tank on the angular motion fixture), but had an even more significant implication. Although it was initially thought that the tank shape and the tank motion independently dictated fluid behavior, the hypothesis, if correct, would couple both effects into a unified and cohesive explanation of how the fluid turbulence is excited.

A test was desired which would convincingly prove or disprove the hypothesis. The angular motion test fixture could not be used because it subjected the tank to rotation about two axes and, therefore, the many variables which affect the liquid's behavior would be difficult to separate. With spin ripple, the linear motion fixture subjected the tank to rotation about the spin axis only. If one rotated the tank by 90° (counterclockwise in Figure 3), so that the cone would point radially out, away from the spin axis, and if the hypothesis were correct, turbulent fluid motion should be observed for the first time on the linear motion test fixture when it had spin ripple. Furthermore, at the limit when the spin ripple is made to disappear (by using the electronic ripple

modulator to offset changes in moment of inertia), the motion should revert to calm rigid-body-type motion.

A series of tests performed on the linear motion test fixture with the tank cone pointed radially out proved the hypothesis to be correct. When the tank exhibited its linear vibrating motion and there was no spin ripple, the fluid was very calm and behaved like a rigid body. As changes were made in the electronic ripple modulator and some ripple was added, the fluid's motion started to change and some rotation of surface particles was evident. As more spin ripple was added, the liquid motion became progressively more turbulent and resembled that observed in the angular motion tests. To obtain further confirmation of the conclusions, the tank was placed in its original position (with the cone axis straight down) and the same tests were repeated. The liquid remained calm and behaved like a rigid body, regardless of the magnitude of the spin ripple.

A possible explanation for this behavior follows. In a nonspinning environment, when one rotates a tank about its symmetry axis, the only forces which the tank exerts on the fluid are shear forces tangential to the moving tank wall. If a tank is rotated about an axis which is not a symmetry axis, the blunt body forces which the tank walls exert on the fluid are trying to change the position and geometry of the fluid. One would expect the fluid's response to these forces to be more energetic, especially in a spinning environment.

## SUMMARY AND CONCLUSIONS

A sphere-cone tank and a spherical tank were subjected to tests on two spin fixtures to investigate the behavior of the liquid under simulated spacecraft motions. The linear motion test fixture subjected the spinning tanks to rectilinear vibration, while the angular motion fixture subjected the spinning tanks to angular oscillations.

Turbulent liquid motion was observed in the spinning INTELSAT IV sphere-cone tank when it was subjected to angular oscillations such as those of a nutating spacecraft. Quantization of the fuel energy dissipation rate by Hughes Aircraft Company [5] led to the incorporation of design modifications on INTELSAT IV to increase the nutational stability margins. The satellite, launched January 25, 1971, has exhibited passive nutational stability in transfer and synchronous orbits.

The principal conclusion derived from the tests is that turbulent liquid motion is excited when a spinning tank is subjected to angular oscillations about an axis which is not parallel to the symmetry axis of the tank. Thus, the liquid in a sphere will dissipate less energy than that in a nonspherical tank; in the Hughes air-ball tests [5] the liquid in the sphere-cone dissipated between 8 and 10 times more energy than the liquid in the sphere.



## REFERENCES


[1] A. J. Iorillo, "Nutation Damping Dynamics of Axisymmetric Rotor Stabilized Satellites," unpublished presentation, *ASME Winter Annual Meeting*, Chicago, Ill., Nov. 1965.

[2] P. W. Likins, "Attitude Stability Criteria for Dual Spin Spacecraft," *Journal of Spacecraft and Rockets*, Vol. 4, No. 12, December 1967, pp. 1638–1643.

[3] C. R. Johnson, "TACSAT I Nutation Dynamics," *AIAA 3rd Communications Satellite Systems Conference*, Los Angeles, Calif., April 1970, AIAA Paper No. 70–455.

[4] E. R. Martin, unpublished paper, April 30, 1971.

[5] Private communications with J. T. Neer, Hughes Aircraft Company.

[6] H. P. Greenspan, *The Theory of Rotating Fluids*, London: Cambridge University Press, 1968.

[7] J. P. Vanyo, "Energy Dissipation in a Liquid Filled Precessing Spherical Cavity and Application to Satellites," Ph.D. dissertation, University of California, Los Angeles, December 1969.

[8] Private communications with P. G. Saffman, California Institute of Technology and H. P. Greenspan, Massachusetts Institute of Technology.


## APPENDIX A

## SPACECRAFT DYNAMIC ANALYSIS

Consider the dual-spin vehicle shown in Figure 2. The rotor angular velocity may be written as

$$\bar{\omega} = \omega_1 \hat{r}_1 + \omega_2 \hat{r}_2 + \omega_3 \hat{r}_3 \tag{A1}$$

where $\hat{r}_1$, $\hat{r}_2$, and $\hat{r}_3$ are body-fixed unit vectors in the direction shown in Figure 2. Similarly, the platform angular velocity is given by

$$\bar{\omega}^P = \omega_1^P \hat{p}_1 + \omega_2^P \hat{p}_2 + \omega_3^P \hat{p}_3 . \tag{A2}$$

The position vector from the origin (spacecraft CG) to the tank center, $Q$, is

$$\bar{r}_Q = a\hat{r}_2 + b\hat{r}_3 . \tag{A3}$$

The linear acceleration of the tank center with respect to an inertial frame is given by

$$\bar{a}_Q = \dot{\bar{\omega}} \times \bar{r}_Q + \bar{\omega} \times (\bar{\omega} \times \bar{r}_Q) \tag{A4}$$

since the tank is in the rotor.

Performing the cross-multiplications and rearranging yields

$$\begin{aligned}\bar{a}_Q = {} & \hat{r}_1(b\dot{\omega}_2 - a\dot{\omega}_3 + a\omega_1\omega_2 + b\omega_1\omega_3) \\ & + \hat{r}_2(b\omega_2\omega_3 - b\dot{\omega}_1 - a\omega_3^2 - a\omega_1^2) \\ & + \hat{r}_3(a\dot{\omega}_1 - b\omega_1^2 - b\omega_2^2 + a\omega_2\omega_3). \end{aligned} \tag{A5}$$

If, at the time $t = 0$, the vector bases, $\hat{p}_1$, $\hat{p}_2$, $\hat{p}_3$ and $\hat{r}_1$, $\hat{r}_2$, $\hat{r}_3$ are coincident, and if

$$\omega_1'(0) = \omega_1(0) = 0$$

$$\omega_2'(0) = \omega_2(0) = \omega_0$$

$$\omega_3'(0) = 0$$

$$\omega_3(0) = \omega_s$$

then

$$\omega_1 = -\omega_0 \sin \lambda' t \tag{A6}$$

$$\omega_2 = \omega_0 \cos \lambda' t \tag{A7}$$

$$\omega_3 = \omega_s \tag{A8}$$

where

$$\omega_0 = \sigma\omega_s \tan\theta \tag{A9}$$

$$\lambda' = (-1 + \sigma)\omega_s \tag{A10}$$

and $\theta$ is the nutation angle.

From equations (A6) through (A8), the acceleration of $Q$ becomes

$$\begin{aligned}\bar{a}_Q = {} & \hat{r}_1(-b\omega_s\lambda' \sin \lambda' t - a\omega_0^2 \sin \lambda' t \cos \lambda' t - b\omega_0\omega_s \sin \lambda' t) \\ & + \hat{r}_2(b\omega_0\omega_s \cos \lambda' t + b\omega_0\lambda' \cos \lambda' t - a\omega_s^2 - a\omega_0^2 \sin^2 \lambda' t) \\ & + \hat{r}_3(-a\omega_0\lambda' \cos \lambda' t - b\omega_0^2 + a\omega_0\omega_s \cos \lambda' t). \end{aligned} \tag{A11}$$

Linearizing in $\omega_0$ yields

$$\begin{aligned}\bar{a}_Q = {} & \hat{r}_1[-b\omega_s(\omega_s + \lambda') \sin \lambda' t] \\ & + \hat{r}_2[b\omega_0(\omega_s + \lambda') \cos \lambda' t - a\omega_s^2] \\ & + \hat{r}_3[a\omega_0(\omega_s - \lambda') \cos \lambda' t]. \end{aligned} \tag{A12}$$

From equation (A10),

$$\omega_s + \lambda' = \sigma\omega_s \tag{A13}$$

$$\omega_s - \lambda' = \omega_s(2 - \sigma). \tag{A14}$$

By substituting these two relationships and the small angle approximation of equation (A9) in equation (A12), we obtain the linearized acceleration equation for $Q$ relative to an inertial frame:

$$\begin{aligned}\bar{a}_Q = {} & \hat{r}_1(-b\sigma^2\omega_s^2\theta \sin \lambda' t) \\ & + \hat{r}_2(b\sigma^2\omega_s^2\theta \cos \lambda' t - a\omega_s^2) \end{aligned}$$



## APPENDIX B

## DYNAMIC ANALYSIS OF LINEAR MOTION FIXTURE

With the tank in its null (undisplaced) position, the original of the body-fixed coordinate system (Figure 3) is arbitrarily chosen at a distance, $b$, above the center of the tank. The angular velocity of the spinning platform is

$$\bar{\omega} = \omega_s\hat{r}_3 . \tag{B1}$$

The motor-cam arrangement drives the tank with an amplitude $X$ and a time function $\cos \lambda' t$. Relative to the body-fixed coordinate system (which is spinning), the instantaneous position vector from 0 to $Q$ is, therefore,

$$\bar{r}_Q = (a - X \cos\psi \cos \lambda' t)\,\hat{r}_2 + (b + X \sin\psi \cos \lambda' t)\,\hat{r}_3 . \tag{B2}$$

The acceleration of the center of the tank as seen from an inertial frame in the absence of gravity is

$$\bar{a}_Q = \ddot{\bar{r}}_Q + \dot{\bar{\omega}} \times \bar{r}_Q + 2\bar{\omega} \times \dot{\bar{r}}_Q + \bar{\omega} \times (\bar{\omega} \times \bar{r}_Q). \tag{B3}$$

Substitution of $\bar{r}_Q$, $\bar{\omega}$ and their derivatives, solution of equation (B3), and linearization of the results yields

$$\begin{aligned}\bar{a}_Q = {} & [-2X\omega_s\lambda' \cos\psi \sin \lambda' t]\,\hat{r}_1 \\ & + [-(\lambda'^2 + \omega_s^2)\,X \cos\psi \cos \lambda' t - a\omega_s^2]\,\hat{r}_2 \\ & + [X\lambda'^2 \sin\psi \cos \lambda' t]\,\hat{r}_3 . \end{aligned} \tag{B4}$$

An observer located at the point $Q$, instead of on an inertial frame, experiences an equal and opposite acceleration which, when gravity is added, is equal to

$$\begin{aligned}g\hat{r}_3 - \bar{a}_Q = {} & [2X\omega_s\lambda' \cos\psi \sin \lambda' t]\,\hat{r}_1 \\ & + [(\lambda'^2 + \omega_s^2)\,X \cos\psi \cos \lambda' t + a\omega_s^2]\,\hat{r}_2 \\ & + [g - X\lambda'^2 \sin\psi \cos \lambda' t]\,\hat{r}_3 . \end{aligned} \tag{B5}$$

## ACKNOWLEDGMENTS

*The laboratory work and the mechanical design of the angular motion test fixture were performed by Mr. Robert E. Ballard. Much of the dynamic analysis presented herein is the work of Mr. Thomas C. Patterson. Other contributors to the program were Dr. Brij Agrawal, Dr. Gary Gordon and Mr. George Huson.*

*I am indebted to Dr. John V. Harrington and Dr. Harold O. Curtis for their suggestions and discussions. Special thanks are due to Mr. John T. Neer of Hughes Aircraft Company for providing access to Hughes data. The cooperation of the COMSAT Project Office for INTELSAT IV is gratefully acknowledged.*

*Ernesto R. Martin has worked in the areas of spacecraft spin stabilization, mechanical devices, and propulsion since he joined the Spacecraft Laboratory at COMSAT Laboratories, Clarksburg, Md., in 1968. His education includes a B.S. in mechanical engineering with high honors from the University of Florida in 1967 and an M.S. in engineering from the California Institute of Technology in 1968. His present interests include advanced stabilization concepts and electric propulsion.*

**Index: bandpass filters, communication satellites, microwave filters, radio transponders**

# NEW TYPES OF WAVEGUIDE BANDPASS FILTERS FOR SATELLITE TRANSPONDERS

A. E. Atia and A. E. Williams

## ABSTRACT

Conventional communications satellite transponder designs employ multiplexing systems based upon Chebycheff or Butterworth waveguide bandpass filters. Not only do these filters represent a significant percentage of the overall transponder weight, but the filtering functions do not possess optimum frequency selectivity, group delay, or in-band insertion loss. This paper describes how the filtering functions can be significantly improved by using orthogonal modes in either square or circular waveguide cavities. Filter weight is reduced by at least 50 percent, and optimum filter functions having flat group delay in the passband and amplitude ripple in both the passband and stopband can be realized. Experimental results obtained from the new types of filters are shown to have superior electrical performance and less weight than comparable conventional Chebycheff waveguide designs.

## INTRODUCTION

High-capacity communication satellite transponders usually require many transmit channelizing filters to distribute the power over the communication band. In order to utilize the allocated frequency spectrum as efficiently as possible, guard bands should be kept very narrow and, hence, sharp cut-off filters are desirable. Further, the filters must have flat in-band group delay and small gain slope in order to minimize distortion and crosstalk [1]. Conventional direct-coupled waveguide Chebycheff filters of high order followed by group-delay equalizers have been used in the design of multiplexing systems for such transponders. For example, the INTELSAT IV multiplexer consists of twelve 36-MHz bandwidth channels, separated center to center by 40 MHz over the 3.7- to 4.2-GHz band. The frequency selectivity of each channel is achieved by a 10-cavity waveguide Chebycheff filter followed by a 5-pole equalizer [2]. These filters constitute a substantial part of the transponder's weight and volume.

This paper describes the theory and design techniques of new types of waveguide filters which possess nearly optimum electrical characteristics and, in addition, weigh significantly less than comparable conventional waveguide filters. The realization of these filters depends